Received: 12 July 2023 | Revised: 19 July 2024 | Accepted: 29 July 2024

DOI: 10.1111/clr.14345

ORIGINAL ARTICLE

CLINICAL ORAL IMPLANTS RESEARCH WILEY

Higher solubility and lower onset temperature of protein denaturation increase the osteoconductive capacity of collagen membranes: A preclinical in vivo study

Zahra Sadat-Marashi[1] | Masako Fujioka-Kobayashi[1,2] | Hiroki Katagiri[3] | Niklaus P. Lang[1] | Nikola Saulacic[1]

[1]Department of Cranio-Maxillofacial Surgery, Faculty of Medicine, Inselspital, Bern University Hospital, University of Bern, Bern, Switzerland

[2]Department of Oral and Maxillofacial Surgery, School of Life Dentistry at Tokyo, The Nippon Dental University, Tokyo, Japan

[3]Advanced Research Center, School of Life Dentistry at Niigata, The Nippon Dental University, Niigata, Japan

Correspondence
Nikola Saulacic, Department of Cranio-Maxillofacial Surgery, Inselspital, Bern University Hospital, Freiburgstrasse 10, Bern 3010, Switzerland.
Email: nikola.saulacic@insel.ch

Funding information
Geistlich Pharma

Abstract

Objectives: Collagen membranes are extensively used for guided bone regeneration procedures, primarily for horizontal bone augmentation. More recently, it has been demonstrated that collagen membranes promote bone regeneration. Present study aimed at assessing if structural modifications of collagen membranes may enhance their osteoconductive capacity.

Methods: Twenty-four adult Wistar rats were used. Bilateral calvaria defects with a diameter of 5 mm were prepared and covered with prototypes of collagen membranes (P1 or P2). The P1 membrane (positive control) presented a lower onset temperature of protein denaturation and a higher solubility than the P2 membrane (test). The contralateral defects were left uncovered (NC). After 1 and 4 weeks, the animals were euthanized. A microcomputed tomography analysis of the harvested samples was performed within and above the bony defect. Undecalcified ground sections were subjected to light microscopy and morphometric analysis.

Results: Bone formation was observed starting from the circumferential borders of the defects in all groups at 1-week of healing. The foci of ossification were observed at the periosteal and *dura mater* sites, with signs of collagen membrane mineralization. However, there was no statistically significant difference between the groups. At 4 weeks, remnants of the collagen fibers were embedded in the newly formed bone. In the P2 group, significantly more bone volume, more new bone, and marrow spaces compared to the NC group were observed. Furthermore, the P2 group showed more bone volume ectocranially then the P1 group.

Conclusions: Bone formation subjacent to a P2 membrane was superior than subjacent to the P1 membrane and significantly better compared to the control. Modifications of the physico-chemical properties may enhance the osteoconductive competence of collagen membranes, supporting bone formation outside the bony defects.

KEYWORDS
bone formation, calvaria, critical-size-defect, histology, micro-CT, morphometry, novel collagen membranes

1 | INTRODUCTION

Reconstruction of bony defects represent a major clinical challenge in craniofacial surgery (Thrivikraman et al., 2017). Owing to its osteoconductivity (Saulacic et al., 2015) and possible osteoinductivity (Miron et al., 2011), autogenous bone is mostly used as a grafting material. Due to a limited quantity of available bone and the morbidity related to the donor site (Scheerlinck et al., 2013), the application of allografts, xenografts, and synthetic biomaterials has been explored for presumptive alternatives for bone grafts in augmentation procedures. The desired characteristic of all bone substitutes is the capacity of osteoconduction, acting as a scaffold for the migration of the cells, their proliferation, and differentiation to promote new bone formation (Thrivikraman et al., 2017). Independent of the grafting material used, the possibility of bone formation in critical-size defect is closely related to the existence of an occlusive barrier membrane (Donos et al., 2004). Guided bone regeneration (GBR) is nowadays the best documented, and the most extensively applied technique in clinical practice for the stimulation of bone augmentation in localized alveolar ridge defects (Benic & Hämmerle, 2014). The concept of GBR is based on the exclusion of connective tissue- and epithelium-derived cells, allowing cells with osteogenic potential to favorably proliferate into the defect (Alberius et al., 1992). Combined application of a bone graft acting as a space maintainer as well as a scaffold for the ingrowth of bone tissue, and a membrane leads to complete integration of the bone graft substitute at the recipient site (Donos et al., 2004; Lundgren et al., 1997; Yip et al., 2015).

Barrier membranes are commonly made of different biocompatible materials that may be divided in biodegradable and non-biodegradable ones, taking the clinical manageability and space-making capacity into consideration (Elgali et al., 2017; Sam & Pillai, 2014). Biodegradable collagen membranes were widely used in peri-implant surgery for the treatment of self-contained bone defects due to their biocompatibility, their capacity of promoting wound healing (Dimitriou et al., 2012; Sbricoli et al., 2020), and their biodegradability rendering removal of the membranes obsolete (Dimitriou et al., 2012; Shin et al., 2018). Previous findings showed that new bone may grow into the rat calvaria defects covered by a collagen membrane only (De Kok et al., 2014; Silva et al., 2017; Song et al., 2014). It is obvious that this healing can only occur if the collagen membrane can act as an osteoconductive scaffold, hereby serving as a mineralization substrate (Strauss et al., 2021). The latter is most likely due to its absorption and accumulation of growth factors released from bone during resorption (Kuchler et al., 2018). Thus, the nature and conformation of the respective collagen molecules may modify the properties of the collagen to support bone formation (Fujioka-Kobayashi et al., 2021; Imber et al., 2021), even though the optimal physicochemical and mechanical properties of the membranes to achieve the best clinical outcomes are still to be established (Omar et al., 2019).

When using the collagen membranes for treatment of self-contained defects, its space-maintaining capacity is of less importance as opposed to treatment of severely atrophied ridges in need of a horizontal and/or vertical ridge augmentation. Under the latter circumstances, membranes not only have to function as space-maintaining barriers for a prolonged time, but also as mechanical stabilizer of the augmented area to prevent displacement of the bone graft. This requires modification of the properties of collagen membranes with regards to their degradation kinetics as well as their mechanical stability. Hence, it is possible that specific modification of the collagen stability may enhance the osteoconductive capacity of a collagen membrane. Fine-tuning the nativity of collagen molecules may pave the way towards tailored collagen membranes (Adamiak & Sionkowska, 2020) suitable for GBR under mechanically challenging conditions.

The present study aimed at assessing the efficacy of two collagen membrane prototypes with different properties in terms of solubility and the onset temperature of protein denaturation to influence healing of critical-size defects in the rat calvaria model. The comparison was between the two prototypes of membranes and an empty control site.

2 | MATERIALS AND METHODS

2.1 | Biomaterials

Two prototypes of sterile, natural, porcine tissue-derived collagen membranes (P1 and P2; Geistlich Pharma AG, Wolhusen, Switzerland) measuring 2.5 × 2.5 cm derived from an intermediate product from routine production of a clinically established collagen membrane (Bio-Gide®, Geistlich Pharma AG, Switzerland) were applied. The P1 membrane served as a positive control, as in vitro and in vivo properties had been previously described (Bozkurt et al., 2014; Caballé-Serrano et al., 2019). The P1 and P2 membranes have been analyzed for chemical composition and the macroscopic characteristics (e.g., thickness, porosity, and surface density).

To assess the state of nativity, the onset temperature of protein denaturation was determined by differential scanning calorimetry (DSC). Punched samples of membranes ($n = 3$) were wetted with phosphate buffered saline (PBS) and incubated at room temperature in aluminum pans; PBS in aluminum pans served as a reference. Three samples were weighed and incubated for 2 days at 37°C in PBS. DSC analysis was performed between 15 and 90°C at intervals of 5°C per minute on a differential scanning calorimeter (Mettler Toledo, OH, USA).

The supernatant was subjected to acidic hydrolysis followed by hydroxyproline quantification by high-performance liquid chromatography (HPLC, Waters). The ratio between extractable and non-extractable proteins was determined based on the hydroxyproline content in the extract and the content of non-extracted samples.

2.2 | Animals

The study was made on 24 male Wistar rats (mean age 14 weeks) approximately 300 g in weight. The animals were housed and fed in

the Central Animal Care Facility at the University of Bern, according to the international standards of animal care, with the temperature adjusted between 19 and 21°C, continuously refreshed air, humidity of 45% ± 10% and a light/dark cycle of 12:12 h. The experimentation followed the NC3Rs, UK guidelines. The protocol was submitted to and approved by the Ethics Committee of the Canton Berne, Switzerland (Nr. BE 68/18) and reported according to the ARRIVE guidelines for preclinical in vivo studies.

2.3 | Surgical procedure

The anesthesia was introduced in an empty induction chamber by inhalation of 600 mL/min O_2 and 8% isoflurane (Forene®, AbbVie Deutschland GmbH & Co. Wiesbaden, Germany). Afterward, the rats were placed in prone position and a non-rebreathable facemask with reduced isoflurane flow of 3%–6% according to the breathing frequency was performed. Before the surgical procedure, the skin calvaria were disinfected using povidone-iodine (Betadine®, MundiPharma Basel, Switzerland). The skin of the calvaria was sectioned sagittally with a no. 15 scalpel, and a local anesthesia was made using Xylocaine Spray 10% (AstraZeneca, Zug, Switzerland). The periosteum was elevated from the original bone surface, and a five-millimeter diameter defect was prepared with a trephine bur under copious irrigation on each side of the parietal bone (Figure 1). Each rat had one application of a prototype collagen membrane (P1 or P2) measuring 7 × 8 mm over the defect without fixation, and, on the contralateral side, an untreated negative control (NC group). Allocation of the treatment was randomized using the software package (www.randomization.com). Flaps were sutured in a double layer with 5-0 Vicryl® (Ethicon, Somerville, NJ, USA) for the periosteum and 5-0 Supramid® (B. Braun Surgical S.A., Rubi, Spain) for the skin. Buprenorphine (Temgesic®, Rechitt Benckiser, Wallisellen, Switzerland) was administered at 0.1 mg/kg s.c. previous to the surgery and every 8 h for 3 days postoperatively.

For the dynamic labeling of bone formation and remodeling, the animals were injected with Tetracycline solution (2%, Sigma Aldrich, Chemie GmbH, Buchs, Switzerland) 25 mg/kg s.c. immediately after surgery, Calcein red (0.6% Calcein/2% $NaHCO_3$, Sigma Aldrich, Chemie GmbH, Buchs, Switzerland) 10 mg/kg i.p. after 2 weeks and Alizarin (30 mg/mL Alizarin R/2% $NaHCO_3$, Sigma Aldrich, Chemie GmbH, Buchs, Switzerland) 30 mg/kg s.c. after 4 weeks, the day before euthanasia.

Animals were euthanatized 1 week (T1) and 4 weeks (T2) after the surgeries by placement in an empty plexyglas box with an overdose of gaseous carbon dioxide. The experimental unit was the animal. No sample size calculation was performed due to the exploratory nature of this study. The primary outcome variable chosen to assess the bone regenerative capacity was the histologically analyzed (two-dimensional) bone volume. In addition, a second method of assessment of the bone regenerative capacity was addressed by microcomputed tomography (μCT). This allowed a three-dimensional evaluation of the bone volume within the total defect and, separately, the superficial osseous coverage of the area.

2.4 | μCT analysis

The collected calvaria specimens were fixed in 10% neutral formalin for 7 days at room temperature and replaced in 70% ethanol at 4°C. The defect sites were subjected to radiography (25 kVP for 10 s) in two projections. The segments were scanned using a high-resolution cone beam scanner (micro-CT 40, ScancoMedical AG, Brüttisellen, Switzerland). The X-ray source (E) was set at 70 kV with 114 μA at high resolution (1000 projections/180°), with a voxel size of 18 μm and an image matrix of 2048–2048 Å pixel. The diameter of the sample holder was 30.7 mm which allowed an increment (resolution) of 15 μm (=voxel size). The integration time was set at 3 s. The μCT slices were reconstructed perpendicularly to the sagittal axis of the calvarium. Mineralized tissue was selected on the greyscale images with the specific threshold set at 220 corresponding to the value of 530 mg HA/cm^3. Voxels above this value could be categorized as mineralized bone or background. The evaluation of the reconstructed 2D images was made with 3D Segmentation of Volume of Interest (Gauss Sigma at 0.8 and Gauss support at 1). Images were reconstructed and analyzed using 3D structural analysis software (Amira, Visualization Sciences Group, Düsseldorf, Germany). The primary volume of interest (VOI_1) was a 5 × 2.5 mm, full thickness cylinder, selected corresponding to the diameter of the defect sites (Figure S1). VOI_1 was further divided into VOI_2 above the bone defect and VOI_3 within the bone defect measuring up to 1.8 and 0.8 mm, respectively (VOI_1 = VOI_2 + VOI_3). The border between VOI_2 and VOI_3 was defined by the upper edges of the bony defect. Segmentation involved thresholding each VOI. Bone volume (BV, mm^3) and bone mineral density (BMD, mgHA/cm^3) were calculated as well. BMD values were normalized against the data from the NC group at the 1-week

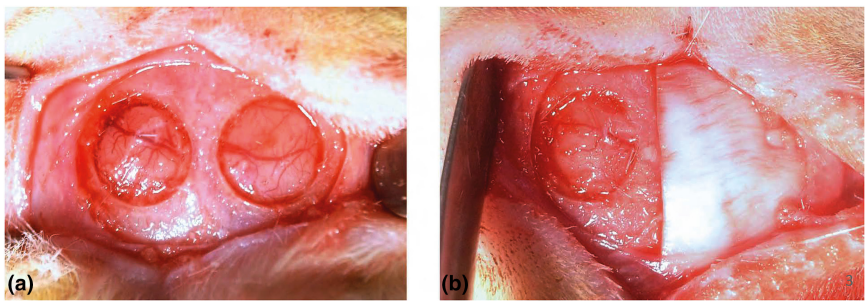

FIGURE 1 Intra-operative view of the exposed rat calvaria. (a) Two 5 mm diameter defects were created in the parietal bone with a trephine drill. (b) Allocated P1 membrane (7 × 8 mm) was placed onto the left defect. The right defect was left untreated.

observation period (internal control, 100%). Hence, values <100% indicated lower BMD relative to an empty defect and values >100% indicated higher BMD relative to an empty defect. Horizontal defect closure (HDC, relative % of the entire defect length) was measured in the VOI_1 at the level of the most prominent bone ingrowth. The most-central, sagittal 2D plane used for the analysis was located at the same distance from the defect borders.

2.5 | Histologic analysis

All specimens were trimmed, and dehydrated using ascending concentrations of ethanol (40%–100%) and xylol and embedded in a methyl methacrylate without decalcification. Five-step serial sections of 1 mm thickness were made by cutting the embedded tissue blocks in the sagittal plane using a slow-speed diamond saw (VC-50; LECO, St. Joseph, MI, USA). The sections were then mounted onto acrylic glass slides, ground, and micro-polished (Knuth-Rotor-3; Struers, Rodovre/Copenhagen, Denmark) to a final thickness of 200 µm. The fluorochrome labeled bone was digitally photographed for tetracycline, alizarin red and calcein green under a light fluorescent microscope (Nikon Eclipse E800; Nikon, Tokyo, Japan). The sections were superficially stained with basic fuchsin and toluidine blue/McNeal, and the images digitally photographed under a light microscope connected to a digital imaging system (VHS-6000, Keyence Japan). Photoshop graphic software (Photoshop CS6; Adobe, San Jose, CA, USA and Olympus CellSens Dimension 1.15, Olympus Corporation, Japan) was used for the histomorphometric analysis of the corresponding 5-mm initial defect area as the region of interest (ROI), corresponding to the VOI (Figure S2). The new bone area (NBA, mm^2) including woven bone, parallel-fibered bone or lamellar bone, bone marrow area (BMA, mm^2) including cells, elements of the extracellular matrix and fat, the residual membrane fibers area (RMA, mm^2) including mineralized and unmineralized fibers, the connective tissue area (CTA, mm^2) except for the above tissues, and the total augmentation area (TAA, mm^2) were assessed at the central sections. Relative area parameters were measured as a % to TAA (NBA/TAA, BMA/TAA, RMA/TAA, and CTA/TAA). For the linear parameters, the horizontal bone defect closure (HDC, %) and the maximum new bone height (NBH, mm) were calculated in the sagittal plane on the third, mid-central sections in all samples. The HDC assessment was performed at the same position histomorphometrically as on the µCT of the corresponding sample.

2.6 | Statistical analysis

The data represented the means and standard deviations (SD) for all quantitative data in tables. A two-way Analysis of Variances (ANOVA) with Tukey test were used to compare the differences between the three groups. A p-value of $<.05$ indicated statistical significance. Statistical analysis was done with the software GraphPad Prism X9 (GraphPad Software, Inc., La Jolla, CA, USA).

3 | RESULTS

3.1 | Biomaterials

The onset temperature of protein denaturation correlated with the natural cross-linking degree after manufacturing and the number of chain scissions introduced during manufacturing and sterilization steps. The two prototype membranes were characterized by differences in solubility and different onset temperatures of protein denaturation. P1, the production of which involved the same processes as the clinically established and commercially available membrane at the laboratory scale presented a lower onset temperature (39°C) and higher solubility (79%) than the P2 membrane (54°C and 2%, respectively; Figure 2). In contrast, the chemical composition (amino acid composition and major proteins) and the macroscopic surface characteristics (thickness, porosity, and material density per surface area) of the P1 and P2 bilayer membranes with an outer, thin, smooth layer and inner, thick, porous layer were proved to be the same (data not shown).

3.2 | Clinical observations

The healing of all sites was uneventful for all 24 animals. No signs of infection or adverse effects appeared. All segments were included in the analysis with $n=12$ for NC group, $n=6$ for P1 group and $n=6$ for P2 group.

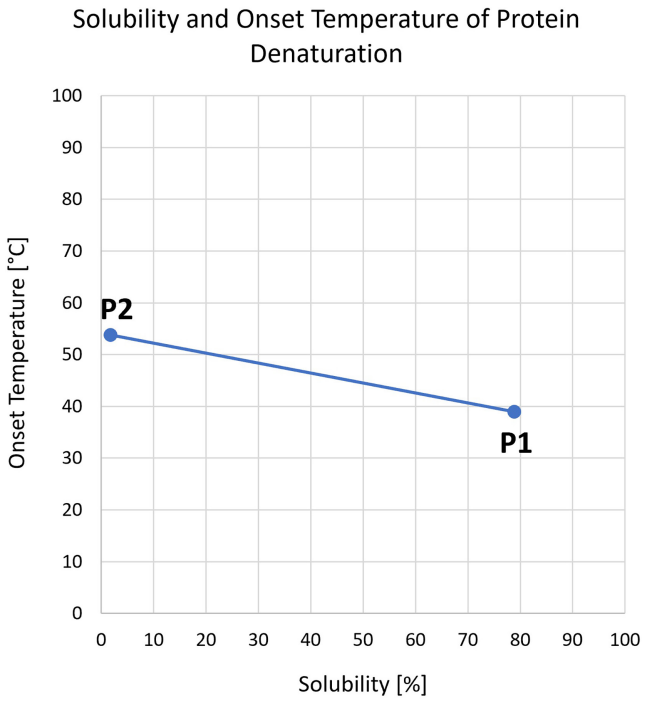

FIGURE 2 Stability and onset temperature of protein degradation for two membrane prototypes P1 and P2.

3.3 | μCT analysis

Bone formation was observed in all defects with both types of prototype membranes (Figure 3). At T1, mineralized tissue was found within the defects originating from the defect border with small, isolated mineralized particles in VOI_2 and VOI_3. However, none of the parameters reached statistical significance differences between the groups (Figure 4, Figure S3). New bone with straight surfaces was observed at T2 in both groups of membranes. Furthermore, some sections of the NC group showed advanced mineralization of the bone defects. Island-like bone formation in VOI_2 was identified in the P1 and NC groups, whereas the areas of bone formation were more pronounced in P2. The BV and BMD values significantly increased from T1 to T2 in all groups in VOI_1 and VOI_3 ($p < .05$, Table S1). Nevertheless, the BMD in NC group increased also in VOI_2 ($p < .05$).

Mineralized tissue at T2 was greater in the P1 and P2 groups when compared to the NC group. The P2 group achieved significantly higher BV values in VOI_1, VOI_2, and VOI_3 in comparison to the NC group, and in VOI_2 compared to the P1 group ($p < .05$; Figure 4; Table S1). However, no significant differences between the groups were observed for the BV/TV (Figure S3). On the other hand, the BMD was higher in the NC than in the P1 and P2 groups in all three VOIs, reaching statistical significance in the VOI_1 ($p < .05$). Significantly higher HDC values were achieved for P2 when compared to the NC group ($p < .05$).

3.4 | Histological analysis

Bone defects preserved the original shape with demarcated borders at T1 (Figure 5). Bone formation was seen at the border of the bone defect and as isolated islands in the middle of the defect. In general, loose connective tissue was found between bone and the membranes. All membranes kept their shapes showing three layers of crisscross-like structures. The P1 samples showed more sparse collagen fibers in the lower part of the membrane, whereas the collagen fibers in the P2 group held more scattered and denser collagen fibers. Osteoid tissue was occasionally observed surrounding the membranes but also infiltrating between the collagen fibers of the membranes (Figure 6a,c). In the P1 and NC groups, bone formation started mainly from the *dura mater* side. In the P2 group, osteoid was growing into the novel membrane from both *dura mater* and periosteal sides as well as in the middle of the membrane. Collagen fibers in both P1 and P2 groups showed signs of mineralization (Figure 6b,e). No significant differences were observed between the groups except for the TAA, being higher for P1 and P2 groups then for the NC group ($p < .05$, Figure 7e, Table S2). On the other hand, the CTA/TAA was significantly higher in the NC group as compared to the P1 and P2 groups (Figure S3).

Bone formation in the defect sites increased from week 1 to week 4 in all samples (Figure 7, Figure S3). The statistically significant difference was reached in P1 and P2 groups for NBA, NBA/TAA, and HDC, and in P2 for BMA, BMA/TAA, and NBH ($p < .05$). Nevertheless, the NC group achieved also a significant difference for NBA/TAA and

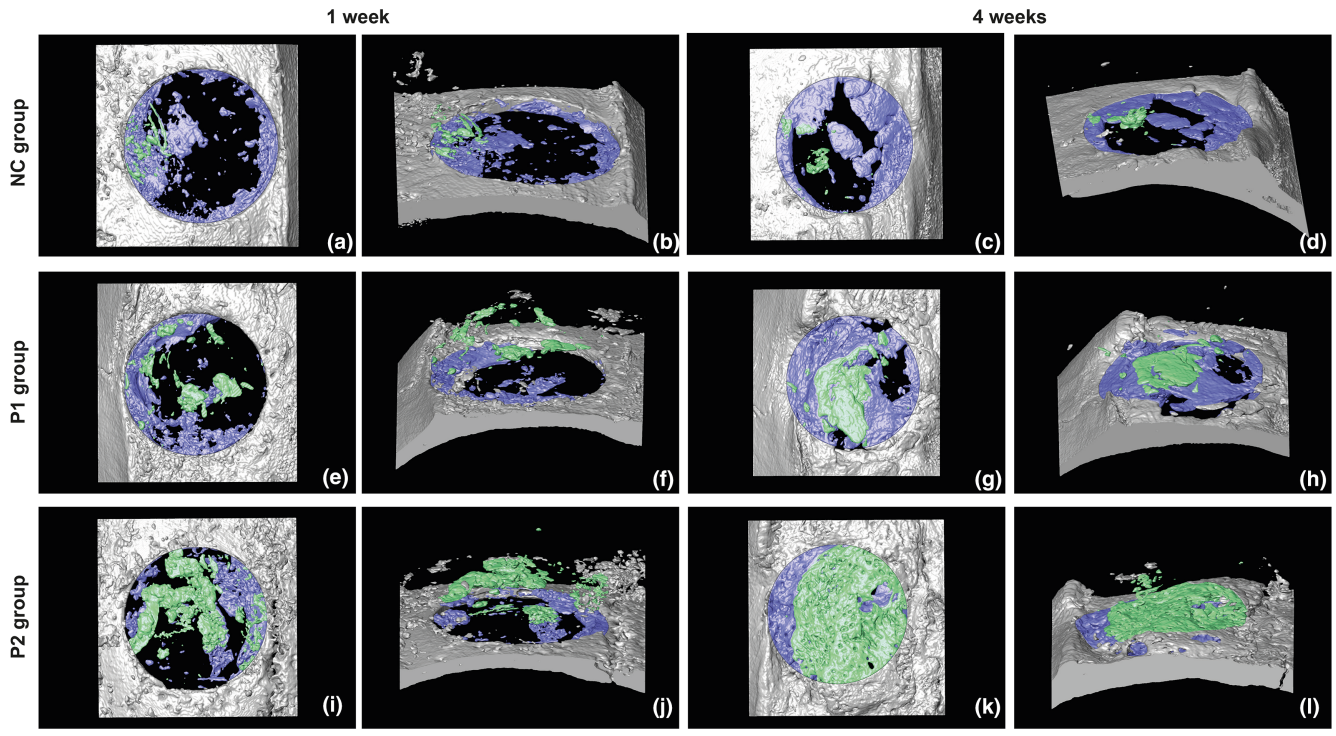

FIGURE 3 Representative 3D radiographs from μCT at 1 and 4 weeks for NC group (a–d), P1 group (e–h), and P2 group (i–l). Light blue is mineralized tissue within the defect (VOI_3) and light green above the defect (VOI_2).

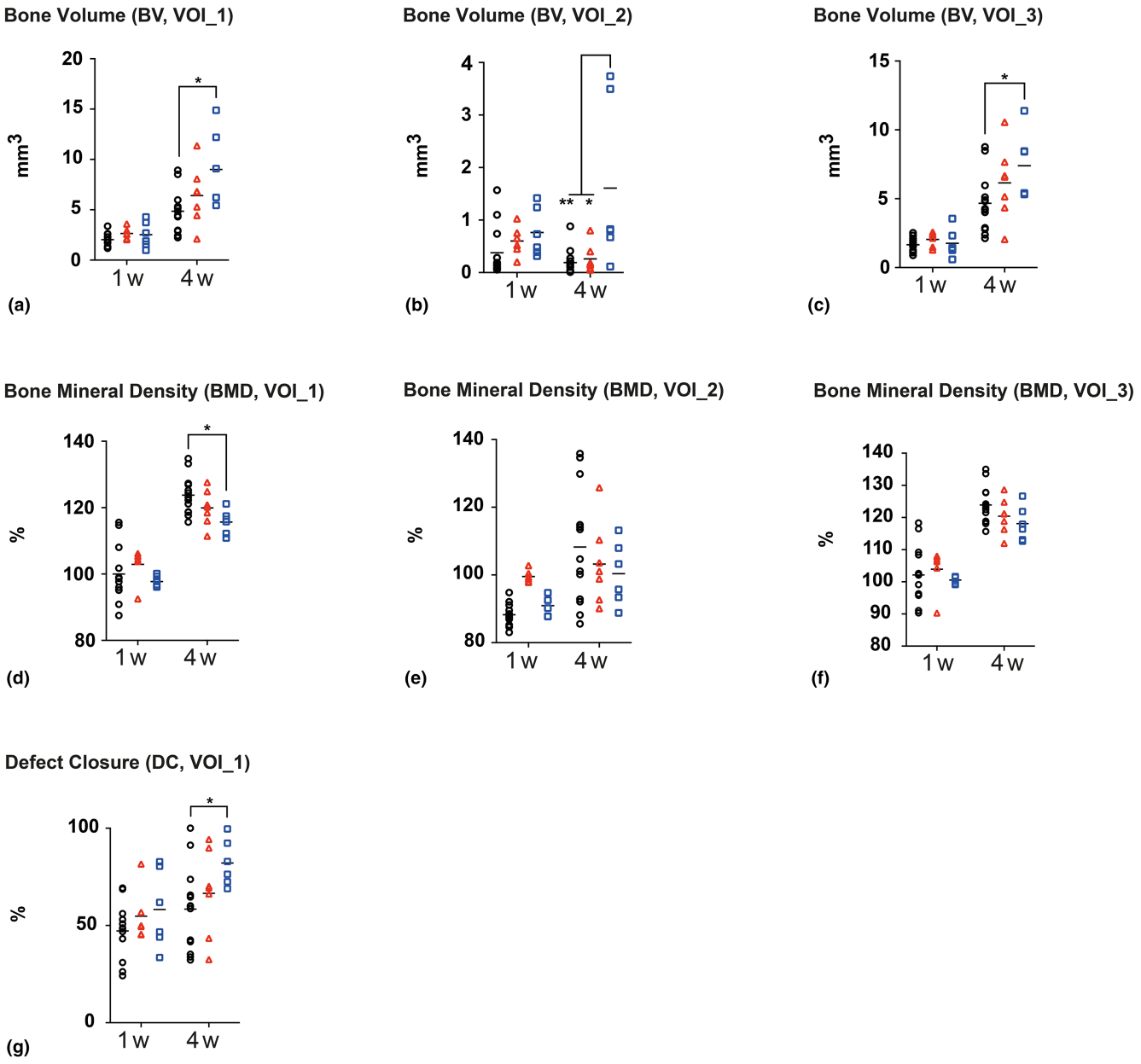

FIGURE 4 μCT radiographic bone volume (BV) in the VOI_1 (a), VOI_2 (b), VOI_3 (c), bone mineral density (BMD) in the VOI_1 (d), VOI_2 (e), VOI_3 (f), and defect closure (DC) in the VOI_1 (g) at 1 and 4 weeks post-surgery. No significant differences between the groups were observed for the BV, BMD and DC at 1-week observation period. P2 group showed more BV compared to NC group at 4-week observation period in VOI_1, VOI_2, and VOI_3, and compared to P1 group in VOI_2. ○□ NC group, △□ P1 group, ▫□ P2 group. Statistically significant differences at $^{*}p < .05$ and $^{**}p < .01$.

BMA/TAA between weeks 1 and 4 ($p < .05$). TAA significantly decreased at T2 as compared to T1 in the P1 group, whereas in the P2 group, it remained unchanged. RMA and RMA/TAA significantly decreased longitudinally in both membrane groups ($p < .05$), whereas the CTA and CTA/TAA decreased in the NC group ($p < .05$).

At T2, new bone originating from the defect borders and isolated bony islands were observed (Figure 5). Bone formation in the NC group, albeit thin, originated from the *dura mater* side (Figure 5j). Tetracycline was not incorporated in the mineralized parts of the membranes in any of the samples. The membranes almost disappeared in both membrane groups, but the remnant collagen fibers with blood vessels within the soft connective tissue in some samples were still present (Figure 6g,j). Fibrous tissue was seen between the remnants of the membranes and the newly formed bone. Calcein labeling disclosed thicker new bone developed from both periosteum and the *dura mater* sides where the defect was covered by the membranes (Figure 5m,q). New bone formed along the remnants of the collagen was more frequently observed in the P1 than in the P2 group. More mature new bone contained light pink fiber-like structures (Figure 6h,k). In the P2 group, signs of bone remodeling with the intervening cell-rich connective tissue were seen. Immature bone and osteoid tissue with areas of

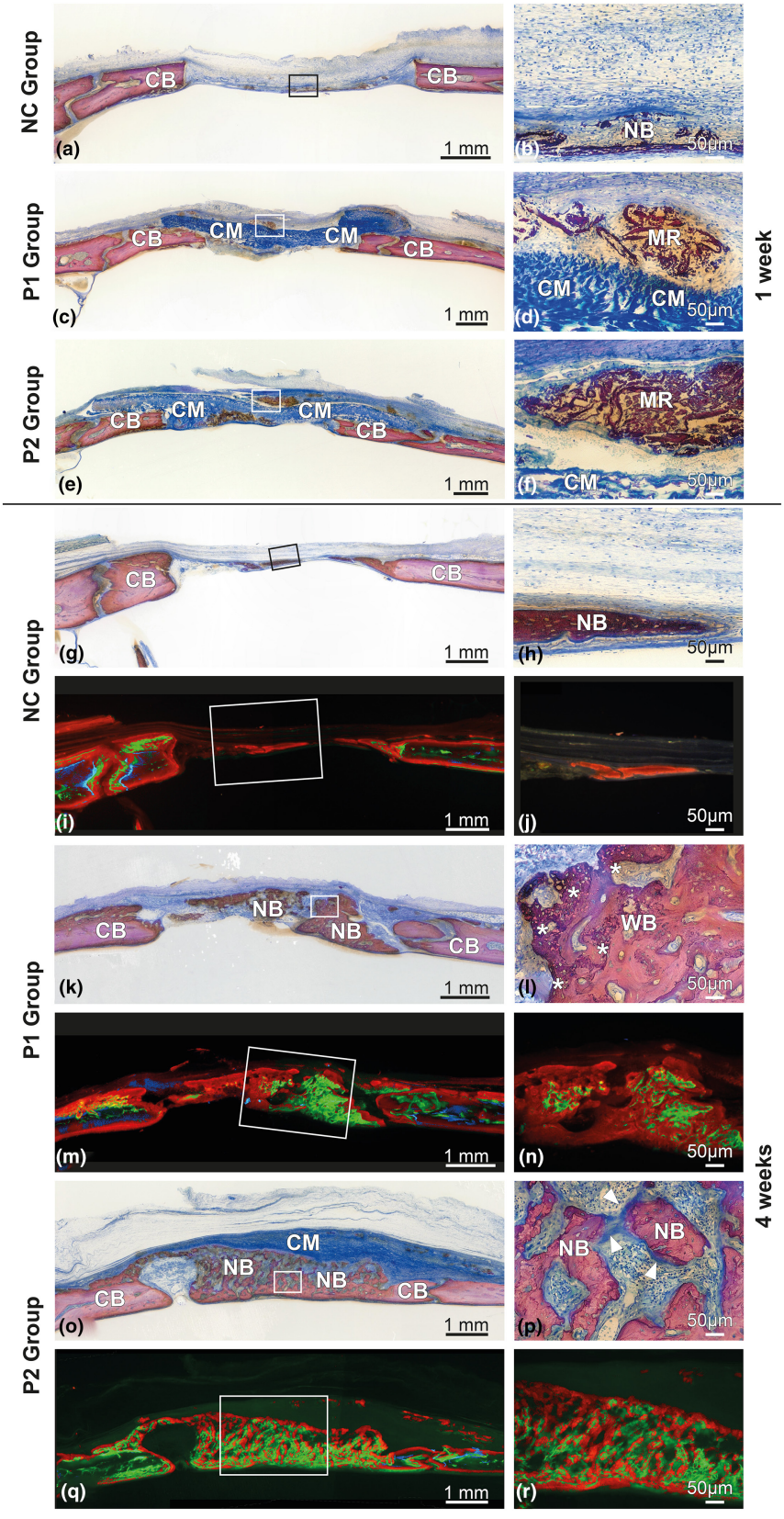

FIGURE 5 Histological view of the defect (sagittal plane) in NC group (a, b, g–j), P1 group (c, d, k–n), and P2 group (e, f, o–r) at 1- and 4-week observation periods. Pristine calvarial bone (CB) demarcates the defect borders at 1-week observation period (a, c, e). Formation of new bone (NB) is restricted to the dura site (b). Dense part of the collagen membrane (CM) is visible overlaying the pristine bone (c, e). Apparently mineralized remnants (MR) of the collagen membrane are indicated by the dark purple stain towards periosteum (d, f). At 4-week observation period, the P1 group (k) and P2 group (o) demonstrated greater bone formation than the NC group (g). Dark staining indicates island of new bone (h). Light pink fiber-like structures (*) present within the woven bone are presumably remnants of the mineralized collagen fibers (l). New bone covered with osteoid (arrowheads) is observed with cell-rich connective tissue (p). Toluidine blue and fuchsin staining. Overviews and magnified views of the merged bone labelling in NC group (i, j), P1 group (m, n), and P2 group (q, r) at 4-week observation period labelled with tetracycline (blue) at 0 week, calcein (green) at 2 weeks, and alizarin (red) at 4 weeks.

mineralization were still recognizable histologically in all groups, especially in the middle of the defect. Less bone formation was generally observed in the NC group; however, a complete bone regeneration was achieved in one sample of this group showing thin bone in the middle of the defect. The P2 group reached statistical significance compared to the NC group for NBA, BMA, HDC, and NBH ($p < .05$; Figure 7). Both P1 and P2 groups showed more CTA and TAA than the NC group ($p < .05$), while the P2 group showed

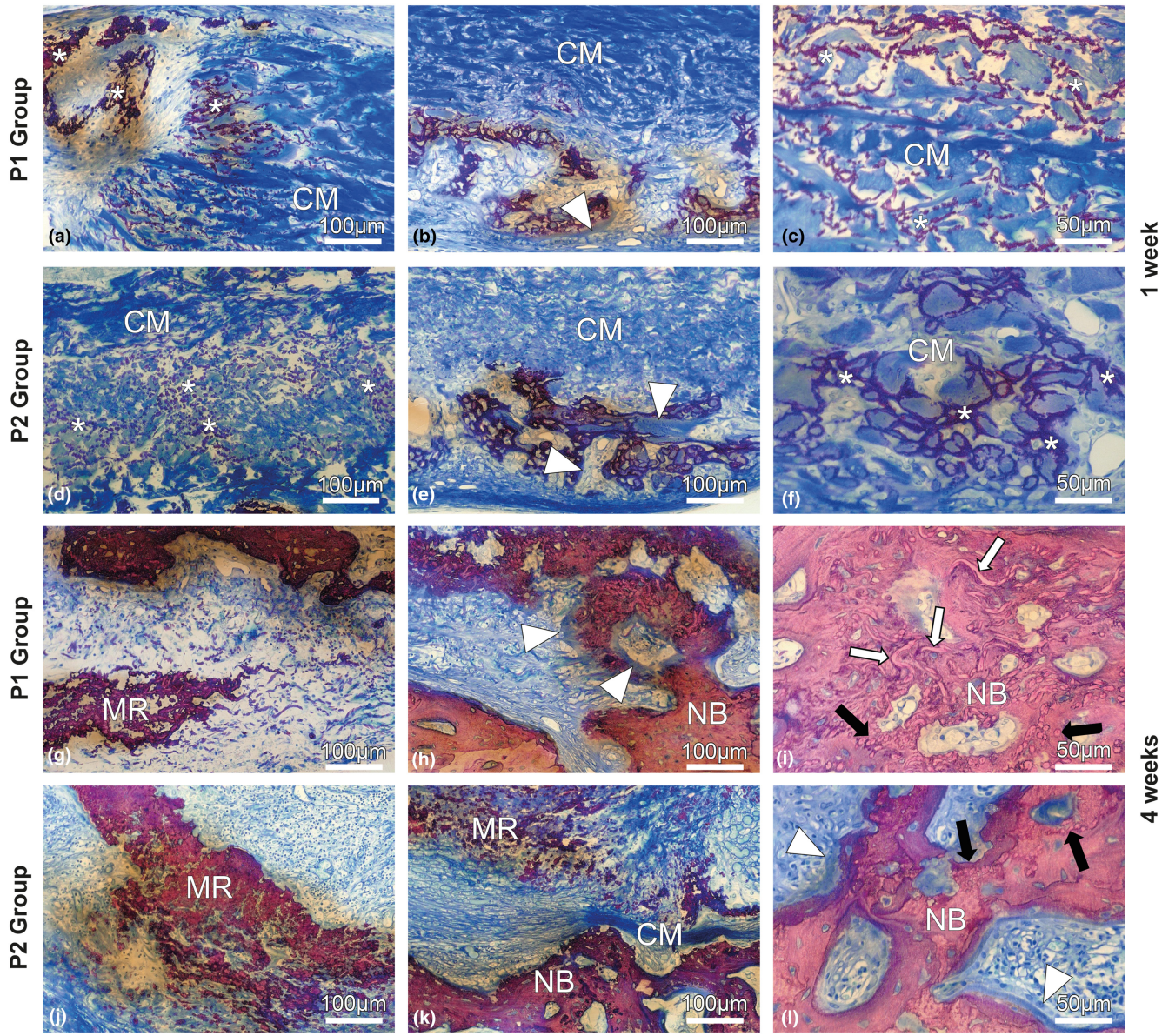

FIGURE 6 High magnification of the histological sections showing collagen membranes (CM) in P1 (a–c, g–i) and P2 groups (d–f, j–l) after 1 and 4 weeks of healing. Pink staining (*) is a mineralization process that proceeds into the space between the collagen fibers at 1-week healing period (a, c, d, f). Characteristic features of immature woven bone indicated by the intense purple stain and the osteoid seams (arrowheads) at the dura sites (b, e). Mineralized remnants (MR) of the fibers in the spongy part of the collagen membranes is seen at 4-week healing period (g, j). The immature newly formed bone (NB) stained in dark purple covered with osteoid is visible in the middle of the defect (h). The new bone with light-pink structures resemble the shape of the collagen fibers in longitudinal (white arrows) and perpendicular orientations (black arrows) (i). The dense outer layer stains positive for purple dye indicating mineralized tissue (k). The dense part of the collagen membrane demarcates the area from the overlying bone. Remnants of the collagen fibers in perpendicular orientation are embedded in the newly formed bone covered with osteoid, with signs of remodeling (l).

more TAA compared to the P1 group ($p < .05$). Nevertheless, no significant differences were observed in relative morphometric parameters between the groups (Figure S3).

4 | DISCUSSION

The present study aimed to evaluate the osteoconductive capacity influenced by two various collagen membrane prototypes using a GBR procedure in a standardized critical-size defect in a rat calvaria model. The P1 membrane was produced by the same manufacturing processes as the clinically established and commercially available collagen membrane. Hence, this P1 membrane was considered as a positive control, while the P2 prototype represented the test. Both membranes were easy to handle and were able to induce new bone formation without signs of a foreign body reactions. The P2, but not the P1 membrane reached a significant difference at T2 compared to the NC group in terms of new bone formation. Modifications of the

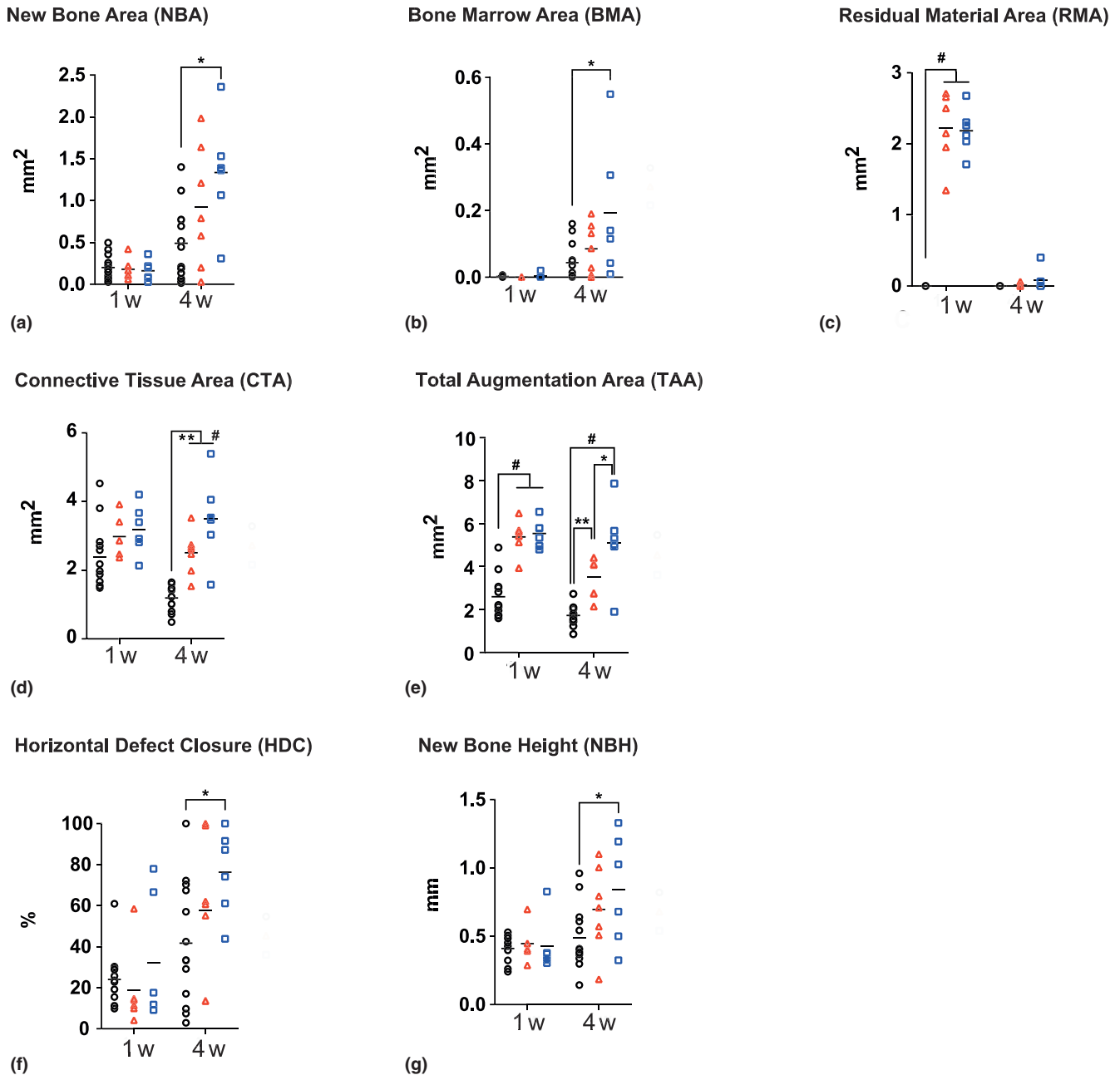

FIGURE 7 Comparison of the histomorphometric results: (a) new bone area (NBA), (b) bone marrow area (BMA), (c) residual material area (RMA), (d) connective tissue area (CTA), (e) total augmentation area (TAA), (f) horizontal defect closure (HDC) and (g) new bone height (NBH). No differences were observed in NBA, BMA, CTA, HDC, and NBH between the groups at 1-week observation period. The P2 groups showed significantly higher values of all morphometric parameters except RMA than the NC group at 4-week observation period. ○□ NC group, △□ P1 group, ▫□ P2 group. Statistically significant differences at $^{*}p < .05$, $^{**}p < .01$, and $^{\#}p < .001$.

physico-chemical properties, as evidenced by the solubility and the onset of protein denaturation temperature enhanced the osteoconductive capacity of the P2.

Osteoblastic cells and newly formed osteoids were observed in all defects including the controls. This bone formation originated from the defect borders, as well as at the periosteal and *dura mater* sites. As previously described, osteoblast progenitor cells contributed to the bone formation at the *dura mater* (Aronin et al., 2008), periosteal (Gruber et al., 2001), and the capillary (Wang et al., 2017) sites. While no significant differences could be recognized at 1week of healing, the 4-week specimens yielded differences in the patterns of bone formation. Both P1 and P2 membranes revealed smooth and rough surface borders. Yet, in agreement with results of previous studies, the wettability (Caballé-Serrano et al., 2019) and cell infiltration (Bozkurt et al., 2014) were not influenced by the surface texture in the present study. Therefore, it is suggested that the osteoconductive properties of the membranes may be influenced by chemical factors released from the defect sites (Kuchler et al., 2018). Furthermore, the collagen membranes appeared to promote the osteogenic differentiation of the resident cells by adsorbing local growth factors belonging to the

transforming growth factor β (TGF-β) superfamily released from the bone matrix (Omar et al., 2019; Strauss et al., 2021). The fixation of the collagen membranes of the bony defects may have enhanced the expression of osteogenic markers and may have supported the formation of newly formed bone (An et al., 2022). These aspects remain to be investigated in future studies. Cell-rich connective tissue surrounded the prototype membranes, whereas the formation of the osteoid tissue was limited to the periphery of the membranes. It may be speculated that the collagen fibers supported migration and growth of mesenchymal cells arising from the bony borders of the defect. In fact, osteoblasts and fibroblasts have been shown to attach to collagen membranes (Behring et al., 2008). Hence, the results of the present study confirmed that the tested prototype collagen membranes may serve as a scaffold for early bone formation (Kuchler et al., 2018; Omar et al., 2019; Strauss et al., 2021). An enhanced protein adsorption may be facilitated by a calcium-binding and mineralization processes (Vo et al., 2015). Shanbhag et al. (2023) demonstrated that mineralization of the collagen fibers proceeded to new bone formation. Calcifying osteoid tissue was distinguishable within and surrounding the membranes. However, the mechanisms of collagen mineralization in these defects are not yet completely understood. As revealed by μCT, signs of ectocranial bone formation with mineralized particles were observed and confirmed the histological analysis. In line with lower solubility and higher onset temperature of protein denaturation, collagen fibers in the P2 group were more distinct, appeared to be sparser and held more cells and osteoid than those subjacent to the P1. However, the only parameter that reached statistical significance at T1 was the TAA, in favor of both prototype membranes compared to the NC group. This was documented by the RMA of about 40% in comparison to the empty control.

Bone formation significantly increased, while the residual biomaterial areas significantly decreased over time in both P1 and P2 groups. Actually, the remnants of the collagen fibers were still visible at T2. The degradation time of the membranes varied according to the type and composition of the collagen used (Sbricoli et al., 2020). Nevertheless, a longer protein degradation time may have interfered with bone formation (Behring et al., 2008). Both the P1 and P2 groups maintained greater bone heights when compared to the NC group, and new bone was thicker than that of the control. Hence, the membranes used in the present study supported bone formation from T1 to T2. The P2 membranes induced significantly higher BV, NBA, BMA, HDC and NBH, and reached statistically significant differences compared to the NC group at T2. The histomophometrical analysis was presented for one region but not for two subregions, as the overall outcome would remain the same. The osteoconductive capacity of collagen membranes may, indeed, be modified by varying their properties. The comparison of the results of the bone volume/area between μCT morphometry and histomorphometry showed similar tendencies. The relative values of newly formed bone demonstrated similar values over the augmentation area among the groups at T2 unlike the absolute values (mm^2/mm^3). The possible explanation is the higher TAA values for the P1 and P2 groups than in the NC group. It is not excluded that the difference in area parameters would have reached statistical significance when related to the ROI, but the fractions of the TAA may be considered more representative for the model used.

According to the μCT findings, two VOIs were defined and analyzed within the defect and ectocranially. The BV increased from T1 to T2 in all groups within the bony defects (VOI_3), where most of the newly formed bone was detected. This corresponded to the findings of Kuchler et al. (2018) and Strauss et al. (2021), who observed bone formation mainly related to the low-density part of the membranes. New bone with embedded collagen fibers showed lower levels of mineralization in comparison to that of the native bone (Shanbhag et al., 2023). The mineralized parts within and at the periphery of the P1 and P2 membranes in the present study showed lower density compared to the control. Inclusion of the membrane parts in the bone volume measurements may explain lower BMD values when compared with the NC group. However, no difference in BMD was observed between P1 and P2. A cell-independent mineralization process may be suggested due to the absence of the osteoblasts (Feher et al., 2021; Kuchler et al., 2018). Still, a light pink fiber-like shape structures embedded in the newly formed bone at T2 probably originated from the collagen fibers (see Figure 5i). While the remodeling on the newly formed bone was seen throughout the bony defects, the osteoid with fibrous structures detected histologically in the center of the defects at T2 indicated an ongoing maturation process. The area measurements of embedded fibers were not performed, as the distinction of their border within the surrounding bone was not always possible. New bone with cell-rich connective tissue with signs of membrane calcification was observed at the *dura mater* sites, and also at the ectocranial part of the membranes at the periosteal site. The ectocranial mineralized particles were remodeled within 3weeks, and smoothly bordered new bone was observed in the defects in the P1 and P2 groups. New bone formation along the remnants of the collagen fibers was more frequently observed in the P1 than in the P2 group. However, the values of the BV in VOI_2 increased only in the P2 group, but the difference did not reach statistical significance compared to T1. Yet, this value was significantly higher in the P2 than in the P1 group at T2. While the bone formation within bone defect was not affected by the type of the membrane, it appeared that the P2 may have supported bone formation even in the ectocranial compartment. This finding might have a clinical relevance, as the membranes are generally placed to cover the bone substitute material outside the bony defects. Collagen membranes may accumulate growth factors released by osteoclasts at the defect sites, and recruit mesenchymal stem cells (Crane & Cao, 2014). According to the location of the ectocranial compartment, it may be assumed that the osteogenic cells originate from the periosteum (Gruber et al., 2001). The exact origin of the cells that contribute to the bone formation still remains to be elucidated.

Collagen has been used for membrane manufacturing in GBR as known to promote wound healing (Bunyaratavej & Wang, 2001). This study confirmed that the clinical relevance of the tested prototype collagen membranes may not be limited to barrier function (Omar et al., 2019). In addition to its semi-occlusive features, prototype collagen membranes may possess osteoconductive competence. Nevertheless, results of the present study have to be related to the critical-size defects in rats. The relatively large intra-group variations in the two test groups reflected the differences in biological responses between the animals. The measurements were consistent

allowing the detection of statistically significant differences in histolomorphometrical and μCT analyses between the groups at T2. The inclusion of later observation periods may be required to complete the remodeling process of the embedded collagen fibers.

Although established as a reproducible model providing reliable outcomes (Delgado-Ruiz et al., 2015), one out of 12 defects in the NC group healed almost completely. A spontaneous regeneration in a critical-size defect (5 mm in rats) may occur in young adult animals. Hence, the age of the animals has to be considered as well, as they may have a higher bone turnover while growing. Yet, the results of the present study should be confirmed in more clinically-relevant models.

5 | CONCLUSIONS

Prototype collagen membranes modified to display distinct physicochemical properties placed to cover bony defects were able to promote bone formation. In this respect, the novel membranes demonstrating a higher onset temperature of protein denaturation, indicative of more intact collagen fibers, induced significantly greater bone formation at 4 weeks compared to the control. The absence of significant differences in the relative area parameters may be explained by the higher TAA values of both P1 and P2. In the rat calvaria defect model, this prototype membrane provided improved outcomes when compared to membrane with lower resorption onset temperature of protein denaturation or an empty control.

AUTHOR CONTRIBUTIONS

Zahra Sadat-Marashi: Writing – original draft; investigation; methodology; validation; formal analysis; data curation. **Masako Fujioka-Kobayashi:** Methodology; data curation; visualization; writing – original draft; validation; investigation. **Hiroki Katagiri:** Writing – original draft; methodology; validation; formal analysis; data curation. **Niklaus P. Lang:** Conceptualization; investigation; funding acquisition; validation; supervision; writing – review and editing. **Nikola Saulacic:** Conceptualization; writing – original draft; writing – review and editing; investigation; funding acquisition; validation; project administration; supervision; data curation.

ACKNOWLEDGMENTS

The authors wish to thank the staff at Central Animal Facilities (CAF), Department of BioMedical Research, University of Bern, Switzerland, for their support of the animal management. We thank Ms. Inga Grigaitiene for her support of histological preparation and histomorphometry. The tested collagen materials were kindly provided by Geistlich Pharma AG (Wolhusen, Switzerland). Open access funding provided by Inselspital Universitatsspital Bern.

FUNDING INFORMATION

This study was supported by Geistlich Pharma AG (Wolhusen, Switzerland).

CONFLICT OF INTEREST STATEMENT

The authors declare that they have no conflict of interest.

DATA AVAILABILITY STATEMENT

The data that support the findings of this study are available from the corresponding author upon reasonable request.

INFORMED CONSENT

Not applicable.

ORCID

Masako Fujioka-Kobayashi https://orcid.org/0000-0002-1511-9085
Hiroki Katagiri https://orcid.org/0000-0002-7464-3274
Niklaus P. Lang https://orcid.org/0000-0002-6938-9611
Nikola Saulacic https://orcid.org/0000-0003-3960-4920

REFERENCES

Adamiak, K., & Sionkowska, A. (2020). Current methods of collagen cross-linking: Review. *International Journal of Biological Macromolecules*, *161*, 550–560. https://doi.org/10.1016/j.ijbiomac.2020.06.075

Alberius, P., Dahlin, C., & Linde, A. (1992). Role of osteopromotion in experimental bone grafting to the skull: A study in adult rats using a membrane technique. *Journal of Oral and Maxillofacial Surgery*, *50*(8), 829–834. https://doi.org/10.1016/0278-2391(92)90274-4

An, Y. Z., Strauss, F. J., Park, J. Y., Shen, Y. Q., Thoma, D. S., & Lee, J. S. (2022). Membrane fixation enhances guided bone regeneration in standardized calvarial defects: A pre-clinical study. *Journal of Clinical Periodontology*, *49*(2), 177–187. https://doi.org/10.1111/jcpe.13583

Aronin, C. P., Cooper, J. A., Jr., Sefcik, L. S., Tholpady, S. S., Ogle, R. C., & Botchwey, E. A. (2008). Osteogenic differentiation of dura mater stem cells cultured in vitro on three-dimensional porous scaffolds of poly (ε-caprolactone) fabricated via co-extrusion and gas foaming. *Acta Biomaterialia*, *4*(5), 1187–1197. https://doi.org/10.1016/j.actbio.2008.02.029

Behring, J., Junker, R., Walboomers, X. F., Chessnut, B., & Jansen, J. A. (2008). Toward guided tissue and bone regeneration: Morphology, attachment, proliferation, and migration of cells cultured on collagen barrier membranes. A systematic review. *Odontology*, *96*(1), 1–11. https://doi.org/10.1007/s10266-008-0087-

Benic, G. I., & Hämmerle, C. H. (2014). Horizontal bone augmentation by means of guided bone regeneration. *Periodontology 2000*, *66*(1), 13–40. https://doi.org/10.1111/prd.12039

Bozkurt, A., Apel, C., Sellhaus, B., van Neerven, S., Wessing, B., Hilgers, R. D., & Pallua, N. (2014). Differences in degradation behavior of two non-cross-linked collagen barrier membranes: An in vitro and in vivo study. *Clinical Oral Implants Research*, *25*(12), 1403–1411. https://doi.org/10.1111/clr.12284

Bunyaratavej, P., & Wang, H. L. (2001). Collagen membranes: A review. *Journal of Periodontology*, *72*(2), 215–229. https://doi.org/10.1902/jop.2001.72.2.215

Caballé-Serrano, J., Munar-Frau, A., Delgado, L., Pérez, R., & Hernández-Alfaro, F. (2019). Physicochemical characterization of barrier membranes for bone regeneration. *Journal of the Mechanical Behavior of Biomedical Materials*, *97*, 13–20. https://doi.org/10.1016/j.jmbbm.2019.04.053

Crane, J. L., & Cao, X. (2014). Bone marrow mesenchymal stem cells and TGF-β signaling in bone remodeling. *The Journal of Clinical Investigation*, *124*(2), 466–472. https://doi.org/10.1172/JCI70050

De Kok, J., Padilla, R. J., & Cooper, F. (2014). Evaluation of a collagen scaffold for cell-based bone repair. *The International Journal of Oral & Maxillofacial Implants*, *29*(1), e122–e129. https://doi.org/10.11607/jomi.te51

Delgado-Ruiz, R. A., Calvo-Guirado, J. L., & Romanos, G. E. (2015). Critical size defects for bone regeneration experiments in rabbit calvariae: Systematic review and quality evaluation using ARRIVE

guidelines. *Clinical Oral Implants Research*, *26*(8), 915–930. https://doi.org/10.1111/clr.12406

Dimitriou, R., Mataliotakis, G. I., Calori, G. M., & Giannoudis, P. V. (2012). The role of barrier membranes for guided bone regeneration and restoration of large bone defects: Current experimental and clinical evidence. *BMC Medicine*, *10*, 81. https://doi.org/10.1186/1741-7015-10-81

Donos, N., Lang, N. P., Karoussis, I. K., Bosshardt, D., Tonetti, M., & Kostopoulos, L. (2004). Effect of GBR in combination with deproteinized bovine bone mineral and/or enamel matrix proteins on the healing of critical-size defects. *Clinical Oral Implants Research*, *15*(1), 101–111. https://doi.org/10.1111/j.1600-0501.2004.00986.x

Elgali, I., Omar, O., Dahlin, C., & Thomsen, P. (2017). Guided bone regeneration: Materials and biological mechanisms revisited. *European Journal of Oral Sciences*, *125*, 315–337. https://doi.org/10.1111/eos.12364

Feher, B., Apaza Alccayhuaman, K. A., Strauss, F. J., Lee, J. S., Tangl, S., Kuchler, U., & Gruber, R. (2021). Osteoconductive properties of upside-down bilayer collagen membranes in rat calvarial defects. *International Journal of Implant Dentistry*, *7*(1), 50. https://doi.org/10.1186/s40729-021-00333-y

Fujioka-Kobayashi, M., Andrejova, E., Katagiri, H., Schaller, B., Sculean, A., Imber, J.-C., Lang, N. P., & Saulacic, N. (2021). Impact of cross-linking of collagen matrices on tissue regeneration in a rabbit Calvarial bone defect. *Materials*, *14*(13), 3740. https://doi.org/10.3390/ma14133740

Gruber, R., Mayer, C., Bobacz, K., Krauth, M. T., Graninger, W., Luyten, F. P., & Erlacher, L. (2001). Effects of cartilage-derived morphogenetic proteins and osteogenic protein-1 on osteochondrogenic differentiation of periosteum-derived cells. *Endocrinology*, *142*(5), 2087–2094. https://doi.org/10.1210/endo.142.5.8163

Imber, J. C., Bosshardt, D. D., Stähli, A., Saulacic, N., Deschner, J., & Sculean, A. (2021). Pre-clinical evaluation of the effect of a volume-stable collagen matrix on periodontal regeneration in two-wall intrabony defects. *Journal of Clinical Periodontology*, *48*(4), 560–569. https://doi.org/10.1111/jcpe.13426

Kuchler, U., Rybaczek, T., Dobask, T., Heimel, P., Tangl, S., Klehm, J., Menzel, M., & Gruber, R. (2018). Bone-conditioned medium modulates the osteoconductive properties of collagen membranes in a rat calvaria defect model. *Clinical Oral Implants Research*, *29*(4), 381–388. https://doi.org/10.1111/clr.13133

Lundgren, A. K., Lundgren, D., Sennerby, L., Taylor, A., Gottlow, J., & Nyman, S. (1997). Augmentation of skull bone using a bioresorbable barrier supported by autologous bone grafts. An intra-individual study in the rabbit. *Clinical Oral Implants Research*, *8*(2), 90–95. https://doi.org/10.1034/j.1600-0501.1997.080203.x

Miron, R. J., Hedbom, E., Saulacic, N., Zhang, Y., Sculean, A., Bosshardt, D. D., & Buser, D. (2011). Osteogenic potential of autogenous bone grafts harvested with four different surgical techniques. *Journal of Dental Research*, *90*(12), 1428–1433. https://doi.org/10.1177/0022034511422718

Omar, O., Elgali, I., Dahlin, C., & Thomsen, P. (2019). Barrier membranes: More than the barrier effect? *Journal of Clinical Periodontology*, *46*(Suppl 21), 103–123. https://doi.org/10.1111/jcpe.13068

Sam, G., & Pillai, B. R. (2014). Evolution of barrier membranes in periodontal regeneration-"are the third generation membranes really here?". *Journal of Clinical and Diagnostic Research: JCDR*, *8*(12), ZE14–ZE17. https://doi.org/10.7860/JCDR/2014/9957.5272

Saulacic, N., Bosshardt, D. D., Jensen, S. S., Miron, R. J., Gruber, R., & Buser, D. (2015). Impact of bone graft harvesting techniques on bone formation and graft resorption: A histomorphometric study in the mandibles of minipigs. *Clinical Oral Implants Research*, *26*(4), 383–391. https://doi.org/10.1111/clr.12357

Sbricoli, L., Guazzo, R., Annunziata, M., Gobbato, L., Bressan, E., & Nastri, L. (2020). Selection of collagen membranes for bone regeneration: A literature review. *Materials (Basel, Switzerland)*, *13*(3), 786. https://doi.org/10.3390/ma13030786

Scheerlinck, L. M., Muradin, M. S., van der Bilt, A., Meijer, G. J., Koole, R., & Van Cann, E. M. (2013). Donor site complications in bone grafting: Comparison of iliac crest, calvarial, and mandibular ramus bone. *The International Journal of Oral & Maxillofacial Implants*, *28*(1), 222–227. https://doi.org/10.11607/jomi.2603

Shanbhag, S., Kampleitner, C., Al-Sharabi, N., Mohamed-Ahmed, S., Apaza Alccayhuaman, K. A., Heimel, P., Tangl, S., Beinlich, A., Rana, N., Sanz, M., Kristoffersen, E. K., Mustafa, K., & Gruber, R. (2023). Functionalizing collagen membranes with MSC-conditioned media promotes guided bone regeneration in rat Calvarial defects. *Cells*, *12*(5), 767. https://doi.org/10.3390/cells12050767

Shin, K., Shihoko, I., Nahoko, K. K., Omori, M., Kayoko, N., Kazuya, I., Yuichi, I., Yoichiro, N., Azumi, H., & Takaaki, U. (2018). Evaluation of guided bone regeneration using the bone substitute bio-Oss and a collagen membrane in a rat cranial bone defect model. *Journal of Hard Tissue Biology*, *27*(1), 85–90. https://doi.org/10.2485/jhtb.27.79

Silva, E. C. E., Omonte, S. V., Martins, A. G. V., de Castro, H. H. O., Gomes, H. E., Zenóbio, É. G., de Oliveira, P. A. D., Horta, M. C. R., & Souza, P. E. A. (2017). Hyaluronic acid on collagen membranes: An experimental study in rats. *Archives of Oral Biology*, *73*, 214–222.

Song, J. M., Shin, S. H., Kim, Y. D., Lee, J. Y., Baek, Y. J., Yoon, S. Y., & Kim, H. S. (2014). Comparative study of chitosan/fibroin–hydroxyapatite and collagen membranes for guided bone regeneration in rat calvarial defects: Micro-computed tomography analysis. *International Journal of Oral Science*, *6*, 87–93. https://doi.org/10.1038/ijos.2014.16

Strauss, F. J., Kuchler, U., Kobatake, R., Heimel, P., Tangl, S., & Gruber, R. (2021). Acid bone lysates reduce bone regeneration in rat calvaria defects. *Journal of Biomedical Materials Research. Part A*, *109*(5), 659–665. https://doi.org/10.1002/jbm.a.37050

Thrivikraman, G., Athirasala, A., Twohig, C., Boda, S. K., & Bertassoni, L. E. (2017). Biomaterials for craniofacial bone regeneration. *Dental Clinics of North America*, *61*(4), 835–856. https://doi.org/10.1016/j.cden.2017.06.003

Vo, T. N., Ekenseair, A. K., Spicer, P. P., Watson, B. M., Tzouanas, S. N., Roh, T. T., & Mikos, A. G. (2015). In vitro and in vivo evaluation of self-mineralization and biocompatibility of injectable, dual-gelling hydrogels for bone tissue engineering. *Journal of Controlled Release: Official Journal of the Controlled Release Society*, *205*, 25–34. https://doi.org/10.1016/j.jconrel.2014.11.028

Wang, J., Gao, Y., Cheng, P., Li, D., Jiang, H., Ji, C., Zhang, S., Shen, C., Li, J., Song, Y., Cao, T., Wang, C., Yang, L., & Pei, G. (2017). CD31hiEmcnhi vessels support new trabecular bone formation at the frontier growth area in the bone defect repair process. *Scientific Reports*, *7*(1), 4990. https://doi.org/10.1038/s41598-017-04150-5

Yip, I., Ma, L., Mattheos, N., Dard, M., & Lang, N. P. (2015). Defect healing with various bone substitutes. *Clinical Oral Implants Research*, *26*, 606–614. https://doi.org/10.1111/clr.12395

SUPPORTING INFORMATION

Additional supporting information can be found online in the Supporting Information section at the end of this article.

How to cite this article: Sadat-Marashi, Z., Fujioka-Kobayashi, M., Katagiri, H., Lang, N. P., & Saulacic, N. (2024). Higher solubility and lower onset temperature of protein denaturation increase the osteoconductive capacity of collagen membranes: A preclinical in vivo study. *Clinical Oral Implants Research*, *35*, 1585–1596. https://doi.org/10.1111/clr.14345